Stress hysteresis as the cause of persistent holes in particulate suspensions

Robert D. Deegan*
Department of Physics and Center for the Study of Complex Systems, Randall Laboratory, University of Michigan, Ann Arbor, Michigan 48109, USA
(Received 22 November 2009; published 26 March 2010)

Concentrated particulate suspensions under vibrations can support stable, localized, vertically oriented free surfaces. The most robust of these structures are persistent holes: deep and stable depressions of the interface. Using a reduced model of the hydrodynamics we show that a rheology with hysteresis can lead to motion opposite to the time-averaged applied force. Moreover, we show experimentally that particulate suspensions of cornstarch in water exhibits hysteresis in the shear-rate response to an applied sinusoidal stress. The results of our model and our experiments suggest that hysteresis accounts for the outward force needed to support persistent holes.

DOI: 10.1103/PhysRevE.81.036319 PACS number(s): 47.20.Ma, 47.50.Gj, 47.54.Jk, 47.57.Qk

I. INTRODUCTION

Particulate suspensions are prevalent in industry, science, and nature. The flow of these fluids is crucial in industries from oil extraction to mining to food preparation, can dramatically affect our environment (e.g., pyroclastic flows) and our health (e.g., blood flow), and continues to draw the interest of researchers. These materials display a variety of non-Newtonian effects and respond nonlinearly at even modest stresses or shear rates. The most salient example of the latter is their propensity at high volume fraction to shear thicken [1]: their apparent viscosity rises with shear rate or stress.

Merkt *et al.* [2] conducted experiments on various concentrated particulate suspensions in a Faraday system. In their experiments, a thin layer, typically 1 cm deep, was vertically vibrated in an open container. They discovered that above a threshold in the acceleration around ten times the acceleration due to gravity, a perturbation of the fluid's free surface nucleated a stable cylindrical void, which extended downward from the free surface through almost the entire layer. These holes persisted indefinitely while the vibration were maintained, but vanished immediate upon the cessation of the vibrations. Merkt *et al.* called these structures *persistent holes*. Schleier-Smith and Stone [3] and Ebata *et al.* [4] found fronts and localized waves similar in nature to persistent holes in vibrated wet granular materials.

Persistent holes display the hallmarks of dissipative solitons in nonequilibrium systems [5]. They are localized structures, and exist only so long as they are supplied with energy. Persistent holes are one of a number of dissipative solitons discovered in the Faraday system. Lioubashevski and coworkers found localized traveling waves in highly viscous fluids [6] and in shear thinning clay suspensions [7]. Umbanhower and co-workers found oscillons in vibrated granular materials [8].

Persistent holes are notably different from other solitons in the Faraday system. Whereas other solitons oscillate about the flat—that is, stable—state, persistent holes oscillate about an unstable configuration. Thus, the stability of persistent holes is puzzling. Despite the hydrostatic pressure gradient pushing fluid into the hole, there is no flow into the hole. Merkt *et al.* [2] tested various other Newtonian and non-Newtonian fluids but were unable to find other complex fluids that supported persistent holes. Based on the latter fact and the typical shear rates observed, Merkt *et al.* concluded that shear thickening is essential for persistent holes.

Here we present the results of our inquiry into the stability of persistent holes. Our approach was to find a reduced model for the coupling of the flow and rheology that reproduced the phenomena. Below we show that a one-dimensional dynamical system with a hysteretic stress-strain rate relation can account for the stability of persistent holes. We further show that the postulated rheology is present in our experimental system. Thus, rather than shear thickening being the root cause of persistent holes as suggested by Merkt *et al.*, we find that hysteresis in the stress response is the key ingredient.

II. METHODS

A. Model

A natural starting point for a model of persistent holes is the incompressible Navier-Stokes equations with an appropriate constitutive relationship. Such an approach is fraught with difficulties because the observed surface profile of the fluid does not naturally conform to any of the usual simplifying approximations (e.g., shallow layer or lubrication), and constitutive relations for dense particulate suspensions are still under development [9–12]. We circumvent these difficulties, at the expense of rigor, by ignoring the continuum aspect of the problem, and developing a one-dimensional model of this phenomenon.

Experiments show that there is no significant exchange of fluid between the annulus of fluid next to the hole and the surrounding fluid [13]. Hence, we model the fluid in the wall of a hole as a block and consider only the horizontal position of its center of mass R. Since experiments show that a furrow is as stable as a cylindrical hole, we neglect the circular symmetry of the hole and treat the block as an isolated mass.

*rddeegan@umich.edu

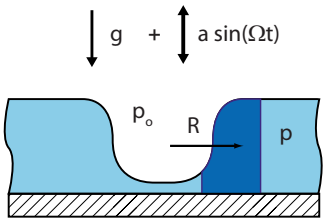

FIG. 1. (Color online) Schematic cross section of a persistent hole. The dark (blue) area is assumed to move as a rigid unit in our model. The driving force comes from the pressure difference between the inside p and the outside p_o. Depending on the instantaneous acceleration, $p > p_o$ for upward acceleration or $p < p_o$ for acceleration downward producing a force to the right or left, respectively. Striped area is the supporting substrate.

Observations of the hole profile show that the walls of the hole oscillate with the period of the drive, growing during the downward acceleration phase and shrinking during the upward phase [2] and that fluid in the walls deforms primarily in shear during this motion. Hence, we approximate the dissipation force on the block by a function of the shear rate $\dot{\gamma}$ and possibly time t. We further assume that the shear rate is proportional to speed of the center of mass $\dot{R}$, where the proportionality constant H has units of inverse length and is of order the boundary layer thickness. As shown in the appendix, the resulting force can be written as $B(\dot{R},t)\dot{R}$.

The external forces on the block of fluid arise from the pressure of the surrounding fluid, and surface tension. We assume that the pressure is dominated by the hydrostatic contribution. As shown in Fig. 1 and in greater detail in the appendix, this gives rise to a horizontal force proportional to the total acceleration. For a sinusoidal drive, the total acceleration is $-g+a \sin \Omega t$, where g is the acceleration due to gravity, and a and Ω are the amplitude and frequency of the applied acceleration. The contribution of surface tension to the pressure is negligible compared to the hydrostatic pressure, and is henceforth ignored. Given these forces and the internal dissipation, the dynamics of the block follows from Newton's law:

$$M\ddot{R} = m(-g + a \sin \Omega t) - B(\dot{R},t)\dot{R}, \tag{1}$$

where M is the mass of the block and m is a constant with units of mass. Introducing the nondimensionalized variables $s=\Omega t$, $u=\frac{M\Omega}{mg}\dot{R}$, $\Gamma=a/g$, and $F=\frac{B\dot{R}}{mg}$, Eq. (1) becomes

$$\frac{du}{ds} = -1 + \Gamma \sin s - F(u,s). \tag{2}$$

B. Rheological measurements

1. Material

Our samples were prepared by mixing cornstarch (Alrich) with a 200.0 mM CsCl aqueous solution in proportions of 3:7 by weight. Cornstarch consists of particles with average radius 5.5 μm. There was no observable swelling of the particles after being immersed in the solution for several days, and thus the volume fraction of the particles is 0.3. The rheological properties of freshly prepared samples drifted as the sample aged, but stabilized after about 48 h. All measurements described below were performed after this transient aging period. A salt solution instead of pure water was used to prevent sedimentation by density matching the granules and the solvent; no visible separation occurred in our samples over a time scale of several days.

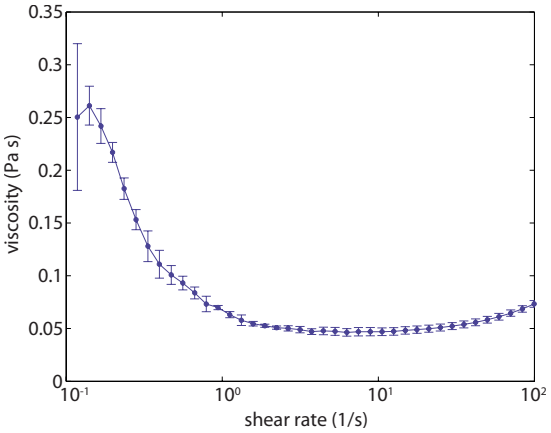

FIG. 2. (Color online) Viscosity of cornstarch solution as measured during an increasing shear stress ramp. The error bars correspond to the observed variation from run-to-run or sample-to-sample.

2. Measurements

Our measurements were done with a stress controlled rheometer (AR-2000ex, TA Instruments) in a cone-plate geometry with an acrylic cone of radius $R_c=3.0$ cm and angle $\alpha = 2° \ 00'$ at 25 °C. Samples were loaded such that the squeezing force during compression of the sample never exceeded 0.1 N. Evaporation was minimized by an enclosure around the test geometry that all but sealed the test fluid from the environment. Steady-state shear viscosity measurements from stress ramps exhibit the characteristic profile of particulate suspensions as shown in Fig. 2: shear thinning for low shear rates followed by shear thickening at higher shear rates [1]. Sequential tests on the same and freshly loaded sample were reproducible to within 10%. Higher shear rates than shown in Fig. 2 produced nonrheometric flows as evidenced by the formation of waves on the meniscus and ultimately to the ejection of the fluid from the geometry. The Peclet number Pe is $\frac{6\pi\eta_s l^3}{kT}\dot{\gamma}$, where kT is the Boltzmann factor and η_s is the solvent viscosity; for these measurements Pe $=780 \ [\mathrm{s}^{-1}]\dot{\gamma}$, which indicates that Brownian motion is negligible even for the lowest shear rates.

Our primary results are from oscillatory stress tests for various stress amplitudes and frequencies. We applied a sinusoidal torque $\tau(t)$ to the test fixture and recorded the angular displacement $\theta(t)$. For frequencies above 0.1 Hz, the combined inertia of the instrument's spindle and the test geometry is a significant factor in the motion. We subtracted this contribution from the applied stress to extract the stress on the material $\sigma(t)$ as follows:

$$\sigma(t) = \frac{3}{2\pi R_c^3}\left[\tau(t) - I\frac{d^2\theta}{dt^2}\right], \tag{3}$$

where I is the total inertia of the apparatus. The shear rate was calculated as $\dot{\gamma}=\cot\alpha\frac{d\theta}{dt}$. There is only a narrow frequency and shear-rate window in which quantitatively reliable data was produced. Wavelike distortions of the meniscus appeared above $\dot{\gamma}\approx 50\ \mathrm{s}^{-1}$, indicating the onset of nonrheometric flows. As the frequency of oscillation increases, the contribution of inertia to the measured torques grows as the frequency squared and ultimately dominates the signal. Extracting the material response from the signal requires differentiating $\theta(t)$ twice with respect to time, an operation that introduces noise. Above 1.0 Hz the material response contribution to the torque is lost in the background of the inertial contribution.

III. RESULTS AND DISCUSSION

A. Model

Below we investigate the dependence of u on the functional form of the frictional force F. A frictional force must be dissipative and its magnitude must be independent of flow direction. Therefore, a physically realistic functional form for F must be such that $F(u)=-F(-u)$ and $\mathrm{sgn}(F)=\mathrm{sgn}(u)$. Furthermore, to ensure mechanical stability (e.g., that flow does not occur spontaneously) we demanded that $\frac{d}{du}F>0$.

The block, as depicted in Fig. 1, represents the right side of the hole. There is also a block that represents the left side. The left block moves as the mirror image of the right block because it experiences a force opposite to the force on the right block. If the two blocks move toward the center and meet, the hole vanishes. Below, where we only specify the motion of the right block, we call motion in the negative direction "closing" because the blocks are approaching each other and the hole is getting smaller. Similarly, motion in the positive direction represents a growing hole, and we call this motion "opening."

For the undriven case, i.e., $\Gamma=0$, the solution to Eq. (2) for arbitrary F is possible. The speed will monotonically approach the limit $F^{-1}(-1)$. As $\frac{d}{du}F>0$, this speed is negative and therefore the hole closes. This result is as expected for any fluid (without a yield stress), including shear thickening fluids: the free surface of a fluid will relax to the flat equilibrium configuration following a disturbance.

For the driven case, i.e., $\Gamma>0$, we consider three classes of rheologies: single-valued time independent, viscoelastic, and hysteretic.

1. Single-valued time-independent case

For $\Gamma>0$ and arbitrary F there is no general analytical solution to Eq. (2). For the Newtonian case $F=bu$, where b is a positive constant, the equation is analytically solvable and yields that the average steady-state speed $\bar{u}=-b^{-1}$. Thus, $\bar{u}<0$ and the solution is closing, in agreement with the experimental observation that Newtonian fluids are unable to sustain holes.

We examined other likely constitutive relations numerically listed in Table I. None produced opening behavior. In all cases and for all tried parameters, $\bar{u}$ was negative. These result are consistent with what one might expect on physical grounds given that the external force $-1+\Gamma\sin t$ averages to -1.

TABLE I. Rheological models. η_1, η_2, η_3, α, β, and $\hat{u}$ are constants that were extensively varied in our simulations.

Model	F/u
Shear thinning	$\eta_1+\eta_2 u^{-\alpha};\ 0<\alpha<1$
Shear thickening	$\eta_1+\eta_2\lvert u\rvert^{\alpha};\ \alpha>0$
Shear thickening and thinning	$\eta_1+\eta_2 u^{-\alpha}+\eta_3\lvert u\rvert^{\beta}$
Discontinuous	η_1 for $\lvert u\rvert<\hat{u}$; η_2 for $\lvert u\rvert\geq\hat{u}$.

2. Linear viscoelastic case

We also examined a linear viscoelastic model. The friction force was evolved according to a Maxwell model,

$$\frac{dF}{dt} = \frac{\beta u - F}{T}, \tag{4}$$

where β and T are constants representing the viscosity and the relaxation time. Differentiating Eq. (2) and substituting Eq. (4) yields

$$\frac{d^2u}{ds^2} + \frac{1}{T}\frac{du}{ds} + \frac{\beta}{T}u = -\frac{1}{T} + \Gamma\left(\cos s + \frac{1}{T}\sin s\right). \tag{5}$$

The solutions is of the form

$$u = \text{"damped term"} + \text{"oscillating term"} - 1 \tag{6}$$

and therefore $\bar{u}=-1$, i.e., a closing solution. Thus, our model with a linear viscoelastic relation is unable to support persistent holes, in agreement with experimental observations [2].

3. Hysteretic case

Motivated by the phenomenological model for suspensions of Head and co-workers [14] that predicted a bistable hysteretic rheology, we used a hysteretic constitutive relation for F. This rheology is able to produce opening solutions. The hysteresis is incorporated by letting $F(u)=b(u)u$ where the damping factor $b(u)$ depends on the history of the sample as follows:

$$b(u) = \begin{cases} b_1 & \text{for when } \lvert u\rvert \text{ falls below } u_1, \\ b_2 & \text{for when } \lvert u\rvert \text{ rises above } u_2. \end{cases} \tag{7}$$

This relationship between the damping force and speed is illustrated in Fig. 3(a).

With this rheological model, Eq. (2) produces both opening and closing type solutions. For $0<\Gamma<1$, the forcing is negative for all times and hence the movement of the block is also always in the negative direction. For $\Gamma>1$, the physical origin of the solutions is illustrated in Figs. 3(b) and 3(c). For low values of $\Gamma>1$ the block only experiences the low damping branch of F. This situation is identical to the New-

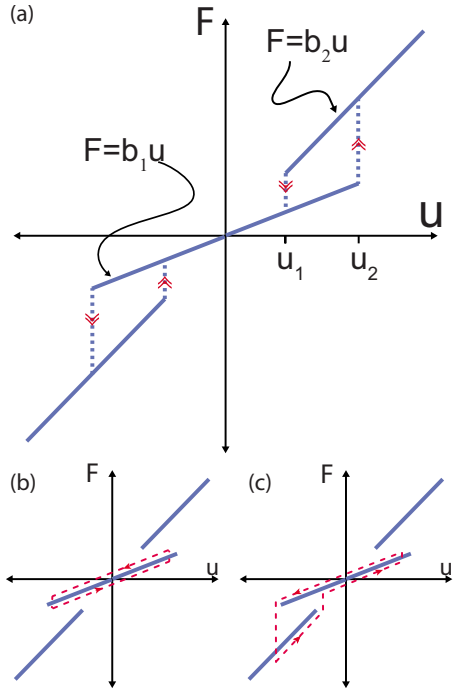

FIG. 3. (Color online) Hysteretic constitutive relation. Solid (blue) lines show the damping force F as a function of u. Dotted (black) lines indicate transitions from the low to high or high to low viscosity branches when $|u|$ exceeds u_2 or falls below u_1, respectively. Dashed (red) line shows velocity history of block during a single cycle below (b) and above (c) the acceleration threshold for opening behavior.

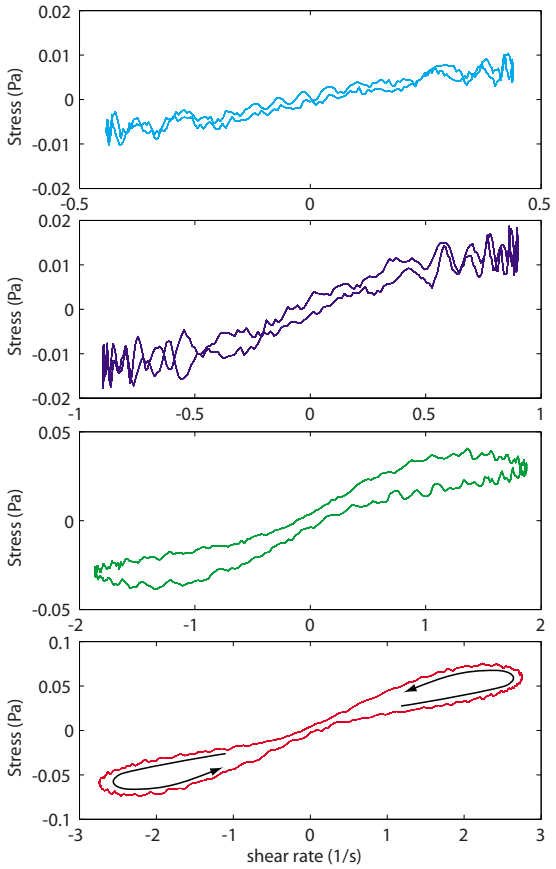

FIG. 4. (Color online) Shear stress σ versus shear rate $\dot{\gamma}$ for an aqueous cornstarch mixture from oscillatory measurements at $\Omega = 3.14$ rad/s for increasing stress amplitude with low at the top. The data, as described in the text, corresponds to the instantaneous values of stress and strain rate during a single oscillation cycle. The arrows indicate increasing phase of the cycle. When the shear-rate increases beyond 1 s^{-1} the curves begin to show a hysteretic response.

tonian case solved above, and produces closing behavior exclusively. This result follows from considering the halves of a full oscillation cycle when the acceleration is positive or negative. During the positive half of the cycle, the average forcing due to acceleration is $-1+2\Gamma/\pi$ and the block slides in the positive direction, while during the negative half of the cycle the average forcing is $-1-2\Gamma/\pi$ and the block slides in the negative direction. Since the total acceleration is greater during the negative half, the total distance moved is greater than during the positive half. During any given cycle, the block moves some in the positive direction but more in the negative direction, and thus the net movement is in the negative or closing direction.

Higher Γ produces higher peak speeds and ultimately the peak speed reaches the transition value $u=u_2$. The block will first encounter this transition point during the negative half of the cycle because the acceleration, and hence the peak speed, is greatest during this half-cycle. Once it reaches this threshold, the system jumps to the higher damping branch, dissipation increases, and the block slows down. Though the block slows down, the system remains on the high damping branch until the speed falls below u_1 because of the hysteresis. The system's excursion through the high damping regime can produce average speeds during the negative half-cycle that are lower than the average speed during the positive half-cycle, and thus the net motion becomes positive and opening solutions occur.

B. Rheology of cornstarch suspension

The hysteretic rheology is the only rheology we found that supports holes. Here we show that a cornstarch suspension that supports persistent holes exhibits hysteresis in oscillatory stress tests. Figure 4 shows a selection of the results at $\Omega=3.14$ rad/s. These measurements were obtained by applying a low pass filter to the raw data, and averaging over 30–50 cycles. Figure 4 is a parametric plot of stress versus the strain rate during a single oscillation cycle. For induced shear rates less than 1 s^{-1}, these curves are essentially single valued. The small enclosed area by these curves is equivalent in magnitude to what we measure for a Newtonian fluid, a glycerol/water mixture, of similar viscosity. Above a shear rate of 1 s^{-1}, the stress response exhibits a qualitative change in character in which hysteresis appears. During the phases when $|\dot{\gamma}|$ is increasing, the stress is lower than during the phases when $|\dot{\gamma}|$ is decreasing. Figure 5 shows similar data to Fig. 4 but for larger torque amplitudes.

We observe hysteresis from our lowest measured frequency 0.628 rad/s up to the maximum frequency that produces reliable data 6.28 rad/s. We also observe hysteresis in

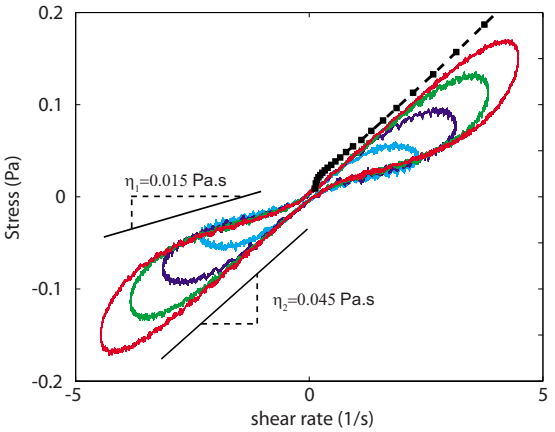

FIG. 5. (Color online) Fig:CompareEtaOscillatory measurements of shear stress σ versus shear rate $\dot{\gamma}$ as in Fig. 4 but for higher stresses. The black squares show the results from a steady shear measurements.

our steady-state measurements between increasing and decreasing stress ramps, and thus, hysteresis may extend to all lower frequencies.

Our rheological measurements are consistent with earlier work in Brownian [15,16] and non-Brownian [17–19] suspensions. These authors observed nonsinusoidal responses to large amplitude sinusoidal drives. The consensus is that these distortions are indicative of the creation and destruction of some microstructure which follows the reversal of flow. We adopt this viewpoint and view our hysteretic rheology as a manifestation of a shear-rate driven first order phase transition from the liquid phase to the structured phase. The latter is consistent with the notion of hydroclusters [20], or the fore-aft asymmetry of experiments [21,22] and Stokesian simulations [23–25].

C. Comparison of rheology, model, and experimental observations

Figure 6 illustrates the similarities and differences of the model and measured rheology. Like the model rheology, our measurements show two distinct responses that are observable when the shear rate exceeds a threshold. For low peak shear rates, $\sigma(\dot{\gamma})$ follows a single curve (denoted "low" in Fig. 6) for increasing and decreasing $\dot{\gamma}$. For an oscillation cycle with a peak shear rates that exceed 1 s^{-1}, $\sigma(\dot{\gamma})$ follows the low branch while $\dot{\gamma}(t) < 1$, then switches to the high branch following a path through the σ-$\dot{\gamma}$ plane that depends on the rate of change of $\dot{\gamma}$. As $\dot{\gamma} \to 0$, there is another transition from the high to the low branch but we are unable to resolve it, though we can say that it occurs before $\dot{\gamma}$ changes sign.

The main differences between the model and measured rheology are that the measured low branch is nonlinear and that the transition from the low to high branch in the measurements displays dynamics not present in the model. The first of these differences is inconsequential; our model can be altered to have a nonlinear shear-rate dependence without changing the qualitative result that opening holes are possible. The second difference cannot be addressed without introducing a more detailed model which accounts for the evolution of the internal state of the fluid. Our preliminary investigations into such a model suggest that the extra detail introduces nothing new.

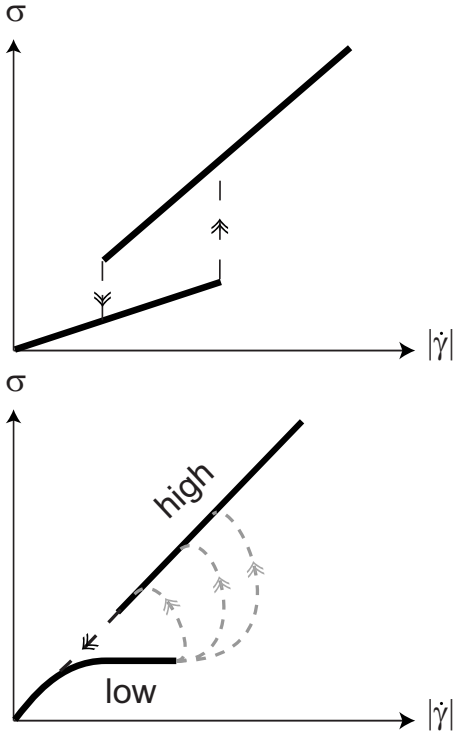

FIG. 6. Schematic comparison of the assumed rheology (top) with the measured rheology (bottom). The dashed lines correspond to transition between the low and high branches.

We now show that the model gives fair quantitative agreement with experimental results assuming that the hysteresis observed at low frequencies persists at higher frequencies. We revisit the latter assumption below. Typical experimental parameters at which persistent holes were observed by Merkt *et al.* are given in Table II: Ω and a are the driving parameters; η_2 and ρ are the material properties where η_2 is taken from the steady-state measurements and ρ is the density; r_1, r_2, h_1, h_2 are the geometrical parameters shown in Fig. 7; and δr is the amplitude of the hole's oscillation during a cycle.

TABLE II. Experimentally parameters for the formation of persistent holes as determined by [2].

Parameter	Value
Ω	942 rad/s
a	15 g
r_1	2.5 mm
r_2	4.5 mm
h_1	1 mm
h_2	5 mm
η_2	50 Poise
ρ	1.7 g/cc
δr	0.35 mm

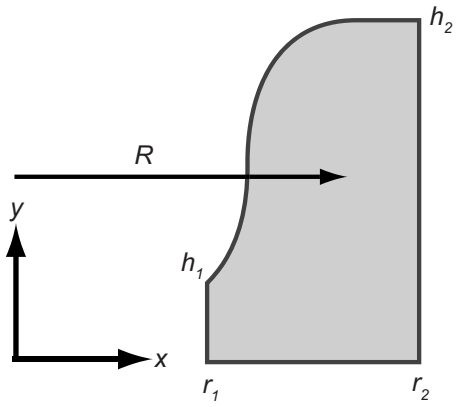

FIG. 7. Fluid mass modeled in Eq. (2)

Combining these parameters into nondimensional forms gives

$$u_2 = \frac{1}{2}\frac{(r_2 - r_1)}{(h_2 - h_1)}\frac{\Omega H}{g}\dot{\gamma}_2 \simeq 6, \tag{8}$$

$$b_2 = \frac{\eta_2}{\rho\Omega H^2} \simeq 5, \tag{9}$$

where we used $\frac{\Omega\delta r}{\sqrt{2}H}$ to compute $\dot{\gamma}$ and assumed that H is the boundary layer thickness $\sqrt{\eta_2/\rho\Omega}$. We assume that $b_1 = b_2/5$ based on the ratio of the high to low viscosity branches in our current measurements. Similarly, we assume that $0 < u_1 \lesssim u_2/10$. The upper and lower limits are based on our observation that $u_2 \gg u_1$ and u_1 is finite. Our model is insensitive to the actual value of u_1 within these limits. Using these parameters and numerically integrating Eq. (2) gives opening solutions for $6.55 < \Gamma < 8.80$, as shown in Fig. 8. This compares favorably, given the approximations of our model, with the measured onset of holes $\Gamma \approx 12$.

The frequencies ranges of the rheological experiments and the experiments showing persistent holes also warrant discussion. The experiment on persistent holes were performed in a range around 100 Hz. Our rheological measurements demonstrating hysteresis in a cornstarch solution were performed at frequencies no higher than 1 Hz. We argue that

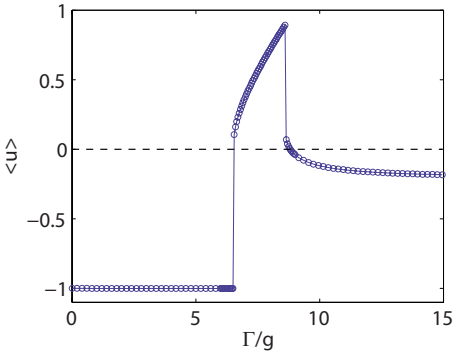

FIG. 8. (Color online) Average velocity computed from Eq. (2) with the hysteretic rheology of Eq. (7) with $u_1=0.6$, $u_2=6$, $b_1=1$, $b_2=5$.

the low frequency response is indicative of the response at the higher frequencies at which persistent holes are observed. Hysteresis is tied to the time scale for the microscopic configuration to reach steady state, as in for example the nucleation of crystallites in a supercooled liquid. In a particulate suspension the time scale associated with the observed hysteresis might be for the formation of hydroclusters. Irrespective of the microscopic origin, the relevant time scale for cornstarch, which are non-Brownian particles, is the inverse shear rate. Thus, provided $\Omega \sim \dot{\gamma}$, or alternatively that the shear $\gamma \sim 1$, hysteresis ought to be present. This is consistent with the observation of holes in which $\gamma \simeq 0.3$.

Lastly, it merits highlighting that the hysteretic force introduced here is meant to answer the question of what could counter the hydrostatic pressure that would cause a hole to collapse in any fluid except particulate suspensions. In particular, our model does not address the finite and preferred size of persistent holes observed in experiments [2]: holes grow without bound in our model. We do not yet know the mechanism which limits the size of the hole. One possibility is that the rise of the liquid layer caused by the hole increases the hydrostatic pressure to the point that it balances the hysteretic force. This effect can be incorporated into Eq. (2) by requiring that h_2 in Eq. (A6) respect conservation of volume. While this clearly a strong effect in some system (e.g., the liquids investigated by [4]), it is less clear in cornstarch solutions which only exhibit a localized rise in the fluid layer.

IV. CONCLUSION

In summary, our study shows that particulate suspensions exhibit hysteresis. Our incorporation of a hysteretic rheology into a minimal model for persistent holes illustrates that hysteresis can generate motion opposite to the time-averaged applied stress. Our block model suggests that hysteresis can account for the wall-like structures observed in vertically oscillated particulate suspensions [2]. Our study has implications for particulate suspensions in particular and complex fluids in general. First, our rheology measurements are consistent with a two-state system with a shear-rate driven transition. The presence of hysteresis implies a time scale for the transformation from one phase to another. Second, our model implies that the anomalous flow found in particulate suspensions might be applicable to complex fluids other than particulate suspensions. Hysteresis is a generic feature of first order phase transitions, and dynamically driven microstructural transitions are common in complex fluids. Hence, it may be profitable to search for similarly unusual flows in complex fluids in the vicinity of microstructural transitions.

ACKNOWLEDGMENTS

We thank Richard Kerswell and Michael Cates for helpful discussions. This material is based upon work supported by the National Science Foundation under Grant No. 0932600

APPENDIX

Consider the block shown in Fig. 7. The block extends L out of the page. We assume that the hydrostatic pressure is

the dominant stress acting on the surface of the block. The horizontal force due to pressure is

$$L\left[\int_0^{h_1} dy\rho\zeta(h_1-y)-\int_0^{h_2} dy\rho\zeta(h_2-y)\right]=-\frac{1}{2}\rho\zeta L(h_2^2-h_1^2), \tag{A1}$$

where ζ is the total acceleration. The rate of energy loss inside the block due to viscosity η is

$$\int dV\sigma\cdot\dot{\gamma}=\eta\overline{\dot{\gamma}^2}V, \tag{A2}$$

where σ is the viscous stress and V is the volume of the block. To rewrite this dissipation in terms of a force $B\dot{R}$ we compare Eq. (A2) with the rate of work due to $B\dot{R}$,

$$\frac{d}{dt}\int_0^x B\dot{R}dx=B\dot{R}^2. \tag{A3}$$

Defining $H\equiv\dot{\gamma}/\dot{R}$, it follows that $B=\frac{\eta V}{H^2}$.

Let M be the mass of the block and R the distance of its center of mass from the origin. Newton's second law gives

$$M\ddot{R}=-B\dot{R}+m\zeta, \tag{A4}$$

where

$$m=\frac{1}{2}\rho L(h_2^2-h_1^2), \tag{A5}$$

$$M=\rho V. \tag{A6}$$

[1] H. A. Barnes, J. Rheol. **33**, 329 (1989).
[2] F. S. Merkt, R. D. Deegan, D. I. Goldman, E. C. Rericha, and H. L. Swinney, Phys. Rev. Lett. **92**, 184501 (2004).
[3] J. M. Schleier-Smith and H. A. Stone, Phys. Rev. Lett. **86**, 3016 (2001).
[4] H. Ebata, S. Tatsumi, and M. Sano, Phys. Rev. E **79**, 066308 (2009).
[5] N. Akhmediev and A. Ankiewicz, *Dissipative solitons* (Springer-Verlag, Berlin, 2005).
[6] O. Lioubashevski, H. Arbell, and J. Fineberg, Phys. Rev. Lett. **76**, 3959 (1996).
[7] O. Lioubashevski and J. Fineberg, Phys. Rev. E **63**, 035302 (2001).
[8] P. B. Umbanhowar, F. Melo, and H. L. Swinney, Nature (London) **382**, 793 (1996).
[9] N. Phan-Thien, X. J. Fan, and B. C. Khoo, Rheol. Acta **38**, 297 (1999).
[10] J. D. Goddard, J. Fluid Mech. **568**, 1 (2006).
[11] J. J. Stickel, R. J. Phillips, and R. L. Powell, J. Rheol. **51**, 1271 (2007).
[12] J. M. Brader, M. E. Cates, and M. Fuchs, Phys. Rev. Lett. **101**, 138301 (2008).
[13] F. S. Merkt, M.S. thesis, University of Texas-Austin, 2003.
[14] D. A. Head, A. Ajdari, and M. E. Cates, Phys. Rev. E **64**, 061509 (2001).
[15] H. M. Laun, R. Bung, and F. Schmidt, J. Rheol. **35**, 999 (1991).
[16] W. H. Boersma, J. Laven, and H. N. Stein, J. Colloid Interface Sci. **149**, 10 (1992).
[17] F. Gadala-Maria and A. Acrivos, J. Rheol. **24**, 799 (1980).
[18] T. Narumi, H. See, A. Suzuki, and T. Hasegawa, J. Rheol. **49**, 71 (2005).
[19] J. M. Bricker and J. E. Butler, J. Rheol. **50**, 711 (2006).
[20] G. Bossis and J. F. Brady, J. Chem. Phys. **91**, 1866 (1989).
[21] V. G. Kolli, E. J. Pollauf, and F. Gadala-Maria, J. Rheol. **46**, 321 (2002).
[22] B. J. Maranzano and N. J. Wagner, J. Chem. Phys. **117**, 10291 (2002).
[23] J. F. Brady and G. Bossis, Annu. Rev. Fluid Mech. **20**, 111 (1988).
[24] J. R. Melrose and R. C. Ball, J. Rheol. **48**, 961 (2004).
[25] S. D. Kulkarni and J. F. Morris, J. Rheol. **53**, 417 (2009).